Progress In Electromagnetics Research, Vol. 123, 105–121, 2012

IMPROVEMENT OF RCS PREDICTION USING MODIFIED ANGULAR DIVISION ALGORITHM

H.-G. Park, K.-K. Park, H.-T. Kim, and K.-T. Kim*

Department of Electrical Engineering, Pohang University of Science & Technology San 31, Hyojadong, Namgu, Pohang, Kyungbuk 790-784, Korea

Abstract—The shooting and bouncing rays (SBR) method has been widely used to predict the radar cross section (RCS) of electrically large and complex targets. SBR computation time rapidly increases as the size and the complexity of a target increase. The angular division algorithm (ADA) can be applied to reduce the number of intersection tests in SBR, which facilitates faster RCS prediction. However, ADA has an error in its table construction step, resulting in incorrect prediction for multiple scattered fields. In this paper, the error is described, and the modified ADA (MADA) is proposed to correct the error and to enhance accuracy. Numerical results show that MADA can achieve good RCS prediction accuracy.

1. INTRODUCTION

High frequency methods can provide fast and robust prediction of radar cross section (RCS) for electrically large targets [1]. Physical optics (PO) can provide reasonable solutions for first-order scattered fields [2], but it cannot consider multiple scattering terms. The shooting and bouncing rays (SBR) method is widely used to calculate multiple scattered fields [3–35]. SBR represents an incident plane wave illuminating the target by a dense grid of ray tubes [3]. To obtain the scattered field, the ray tubes are traced until there is no reflection from the target, and then the physical optics integral [2] is performed on the exit position. RCS prediction using SBR is accurate for electrically large and complex targets. In SBR, the density of incident ray tubes should be greater than ten ray tubes per wavelength to make

Received 13 October 2011, Accepted 30 November 2011, Scheduled 14 December 2011

* Corresponding author: Kyung-Tae Kim (kkt@postech.ac.kr).

results convergent [3]. Hence, SBR requires huge calculation times for electrically large targets because its computational complexity is proportional to the number of incident ray tubes. Moreover, the calculation time increases as the number of facets in the target model increases because the number of intersection tests per ray tube is directly proportional to the number of facets.

Numerous techniques have been proposed to accelerate SBR by reducing those two factors [4–27]: the number of incident ray tubes and the number of intersection tests per ray tubes. The multiresolution grid algorithm in SBR (MSBR) was proposed to reduce the number of incident ray tubes by using relatively larger incident ray tubes than those of SBR [4]. Furthermore, MSBR was further improved by using a graphics processing unit [5]. Latterly, beam tracing [6–12] was applied to RCS predictions. In general, beam tracing requires less incident ray tubes than conventional SBR for electrically large targets [6, 7].

To decrease the number of intersection tests per ray tube, space division algorithms, such as the kd-tree [13, 14] and the octree structure [15, 16], were applied to SBR, and MSBR and the octree were also combined for SBR acceleration [17]. The angular z-buffer (AZB) algorithm was proposed to reduce the number of intersection tests in ray tracing. AZB is widely used to accelerate ray tracing and provides efficient solutions for the UHF-propagation problems in particular [18–20]. Recently, the angular division algorithm (ADA) [21, 22] was proposed which can provide an efficient RCS prediction by reducing the computational complexity in the intersection tests. Although ADA has some similarities to AZB, ADA has a certain difference that makes it especially well suited for RCS predictions. AZB generates N_a angular regions called *anxels* for a source and finds facets in each anxel. The facets stored in these anxels are candidates for being "first-order reflected facets". AZB can consider nth-order reflections by making additional anxels for every "$(n-1)$th-order reflection facets" using the image method. As higher-order reflections are considered, the computational cost to generate anxels increases, but the information in the anxels decreases [18]. This reduces the efficiency of AZB for high-order reflection cases. Like AZB, ADA generates N_a angular regions for every facet in the target model. However, facets stored in the angular regions for facet A could be "next-order reflected facets after reflection from facet A". ADA can reduce the number of candidate facets for each intersection test and has the same efficiency regardless of the reflection order. Therefore, ADA may be suitable for RCS predictions that require many ray tracing processes due to multiple reflections [21].

Although the conventional ADA is computationally efficient like AZB, it has some RCS accuracy problems due to its erroneous

estimation of θ angle. In Section 2, we describe the drawback of the conventional ADA that can degrade accuracy of RCS prediction. A new method called modified ADA (MADA) to overcome the demerit of the conventional ADA is introduced in Section 3, and several RCS prediction examples to demonstrate the proposed MADA are presented in Section 4.

2. DRAWBACK OF THE CONVENTIONAL ADA

Conventional SBR performs intersection tests for each ray with all facets modeling the target. These tests between ray and facets should be recursively carried out to obtain scattered fields. As the size and the complexity of targets increase, the number of intersection tests rapidly increases, leading to huge computation times. To decrease the computational complexity, ADA has been applied to the conventional SBR [21, 22]. ADA generates N_a angular regions for each facet in the target model, i.e., each reference facet. The relative facets, all other facets except for a given reference facet, are arranged in the angular regions of the reference facet according to their angular range relative to the reference facet, the maximum and the minimum ϕ and θ angles in spherical coordinates. For example, the relative facet with maximum and the minimum ϕ and θ angles $\phi_{\max}$, $\phi_{\min}$, $\theta_{\max}$, and $\theta_{\min}$ is located in angular regions 6, 7, 10, and 11 (Figure 1). These arrangements are stored in the distribution information table (DIT) in advance of the main ray tracing procedure. ADA finds the angular region where a ray reflected from the reference facet propagates by using the ϕ and θ angles of the ray and then performs the intersection tests with only facets arranged in that angular region. ADA can significantly reduce

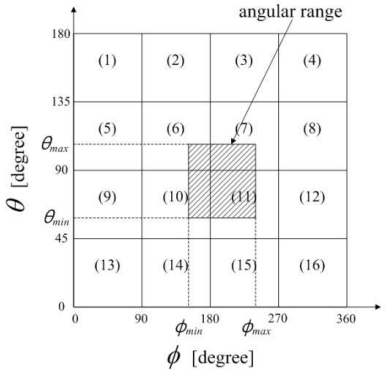

Figure 1. Angular regions: regions are labeled with index numbers.

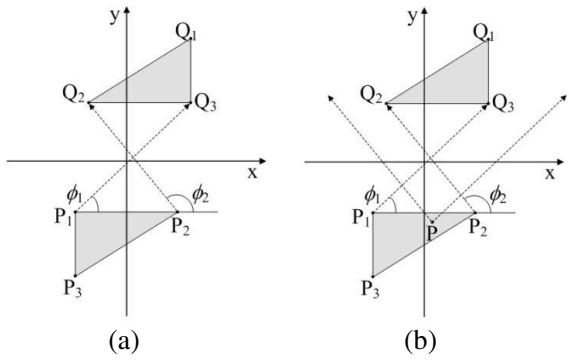

Figure 2. Two-dimensional description of the ϕ range between two facets.

the number of intersection tests required in conventional SBR [21, 22].

ADA obtains the maximum and the minimum ϕ and θ angles between the reference facet and the relative facet by using the nine vectors between the vertices of each facet for targets modeled with triangular facets [21, 22]. For example, consider two facets, the reference facet $P_1P_2P_3$ and the relative facet $Q_1Q_2Q_3$. ADA calculates the ϕ and θ angles of nine vectors, $\overrightarrow{P_1Q_1}$, $\overrightarrow{P_1Q_2}$, $\overrightarrow{P_1Q_3}$, $\overrightarrow{P_2Q_1}$, $\overrightarrow{P_2Q_2}$, $\overrightarrow{P_2Q_3}$, $\overrightarrow{P_3Q_1}$, $\overrightarrow{P_3Q_2}$, and $\overrightarrow{P_3Q_3}$, and the maximum and minimum angle values are obtained by comparing those values.

The maximum and minimum ϕ angles calculated by the above method can correctly define the ϕ-range between the two facets. All rays reflected from the reference facet and hitting the relative facet have ϕ values between these maximum and minimum ϕ angles. In Figure 2, $P_1P_2P_3$ and $Q_1Q_2Q_3$ represent the orthogonal projections of the reference facet and the relative facet onto the x-y plane, respectively. Because the ϕ angles are calculated from only x and y, the two-dimensional description in Figure 2 can be valid. ADA calculates the maximum ϕ as ϕ_2 from $\overrightarrow{P_2Q_2}$ and the minimum as ϕ_1 from $\overrightarrow{P_1Q_3}$ (Figure 2(a)). For any point P on the reference facet, Figure 2(b) clearly shows that a ray transmitted from P should have ϕ value between ϕ_1 and ϕ_2 for the ray to hit the relative facet.

However, an error in θ values may occur because equivalent θ-planes have conical shapes and modeling facets have planar surfaces [20] (Figure 3). As mentioned previously, ADA calculates the θ values by using vectors from vertices of the reference facet to vertices of the relative facet. For example, let the point O be one

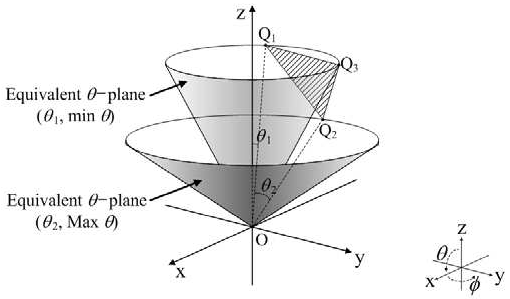

Figure 3. Equivalent θ-planes.

vertex of the reference facet and $Q_1Q_2Q_3$ be a relative facet (Figure 3). ADA calculates the maximum θ as θ_2 from $\overrightarrow{O_2Q_2}$ and the minimum as θ_1 from $\overrightarrow{OQ_1}$ or $\overrightarrow{O_2Q_3}$. However, all points on the line segment Q_1Q_3 except Q_1 and Q_3 have smaller θ values than the minimum θ_1 estimated using ADA, as clearly shown in Figure 3. In other words, the line segment Q_1Q_3 exists above the equivalent θ-plane corresponding to the minimum θ_1. These incorrect θ values in ADA can result in an inaccurate DIT. An error in DIT can cause ray-misses for multiple reflections, leading to RCS prediction errors.

Saeidi and Hodjatkashani presented an efficient remedy for the above θ problems between a point source and a planar facet [20]. They presented a mathematical solution for the maximum and minimum θ values between a point and a line segment. In addition, their solution can provide correct maximum and minimum θ values between a point and an arbitrary planar facet in a three-dimensional space.

However, Saeidi's method cannot be directly applied to ADA, because ADA is based on the maximum and minimum angles between two facets, rather than between a point and a facet. This is due to the fact that ADA's extremum angles between two facets are affected by the positions of two points on two different planar facets simultaneously.

3. MODIFIED ADA

We propose a MADA to remedy the ray-miss problems of the conventional ADA caused by the incorrect θ values mentioned in Section 2. The conventional ADA defines the angular regions by $\max(\theta, \phi)$ and $\min(\theta, \phi)$ (Figure 4(a)) [21, 22]. A typical example of the $\max(\theta, \phi)$ and $\min(\theta, \phi)$ for each angular region in ADA is shown

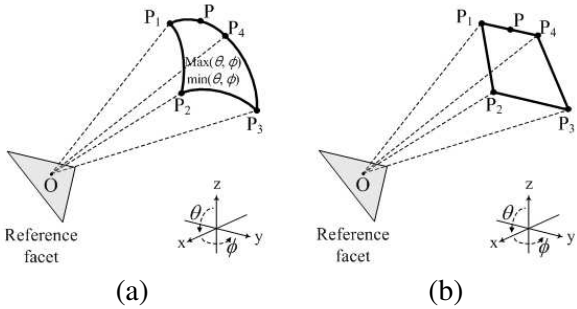

Figure 4. Definition of an angular region: (a) ADA and (b) MADA.

in Figure 1. Specifically, the angular region labeled 7 in Figure 1 has $\max(\theta, \phi) = (135°, 270°)$ and $\min(\theta, \phi) = (90°, 180°)$. However, the angular regions of MADA are defined as a pyramidal region surrounded by four edge planes. The modified angular region of MADA is defined by four edge planes, $\mathrm{OP_1P_2}$, $\mathrm{OP_2P_3}$, $\mathrm{OP_3P_4}$, and $\mathrm{OP_4P_1}$ (Figure 4(b)). Four unit vectors, $\overrightarrow{\mathrm{OP_1}}$, $\overrightarrow{\mathrm{OP_2}}$, $\overrightarrow{\mathrm{OP_3}}$, and $\overrightarrow{\mathrm{OP_4}}$, can be obtained using the $\max(\theta, \phi)$ and $\min(\theta, \phi)$ of the angular region of the conventional ADA. For example, $\overrightarrow{\mathrm{OP_1}}$ shown in Figure 4 is a vector of $(1, \min\theta, \max\phi)$ in spherical coordinates. Angular regions of MADA are the same as those of conventional ADA in terms of ϕ, but different in terms of θ, due to their planar boundaries. For any point P on the upper or lower boundary of the angular region, $\overrightarrow{\mathrm{OP}}$ has the same θ value as the unit corner vector, $\overrightarrow{\mathrm{OP_1}}$, $\overrightarrow{\mathrm{OP_2}}$, $\overrightarrow{\mathrm{OP_3}}$, or $\overrightarrow{\mathrm{OP_4}}$, in ADA, but not in MADA. For example, in ADA (Figure 4(a)), for a point P, the middle point of the circular arc $\mathrm{P_1P_4}$, θ value of $\overrightarrow{\mathrm{OP}}$ is the same as that of $\overrightarrow{\mathrm{OP_1}}$ and $\overrightarrow{\mathrm{OP_4}}$. In MADA (Figure 4(b)), however, for a point P, the middle point of the line segment $\overrightarrow{\mathrm{P_1P_4}}$, θ value of $\overrightarrow{\mathrm{OP}}$ is different from that of $\overrightarrow{\mathrm{OP_1}}$ and $\overrightarrow{\mathrm{OP_4}}$, as illustrated in Figure 3.

The conventional ADA arranges the relative facets into angular regions according to the relative angular range between the reference and the relative facets (Figure 1). On the other hand, MADA generates N_a angular regions of the reference facet in three-dimensional space and arranges the relative facets into those angular regions according to existence of the relative facets in the angular regions. For a ray reflected from the ith reference facet and whose direction vector heads toward the jth angular region, the modified angular region of the reference facet in three-dimensional space, MAR_{ij}, covers a whole space

into which the reflected ray can propagate. MAR_{ij} can be obtained as follows (Figure 5):

1) Position the origin O of the angular region at any vertex of the reference facet.

2) Move the angular region along three sides of the reference facet.

3) Find the outermost edge planes, $a_m x + b_m y + c_m z + d_m = 0$ ($m = 1, 2, \ldots, N_p$, where N_p is the number of outermost edge planes), of the volume generated by moving the angular region. Normal vectors of the outermost edge planes, $\hat{n}_m = (a_m, b_m, c_m)$, head toward the outside of the volume.

4) Define MAR_{ij} as the space surrounded by those outermost edge planes.

In MADA, the reflected ray propagation space can be exactly defined by MAR_{ij}. We propose a modified DIT (MDIT) based

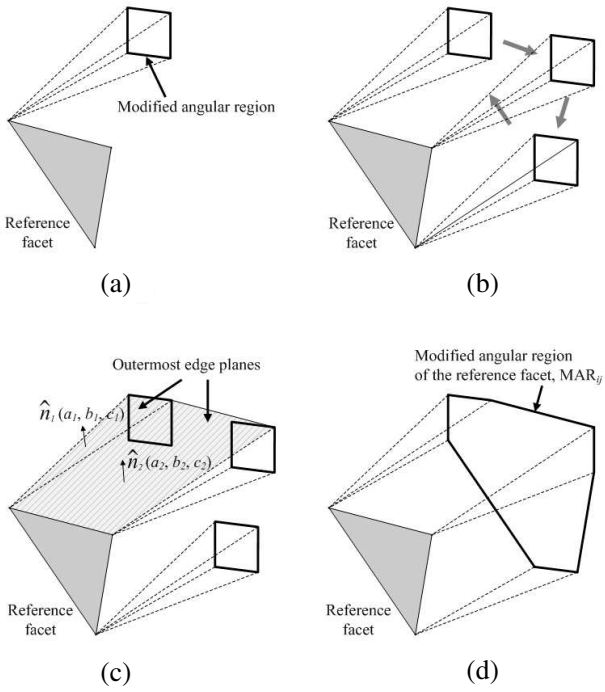

Figure 5. Schematic representation for the procedure to generate an angular region of the reference facet: (a) step 1, (b) step 2, (c) step 3, and (d) step 4.

on MAR_{ij} to solve the accuracy problem of the conventional ADA. Construction of the proposed MDIT depends only on the existence of facets in the region, unlike the conventional DIT of ADA using incorrect relative angular positions between reference and relative facets, as mentioned in Section 2. Therefore, MADA has no ray-miss problem and can provide accurate RCS predictions. The MDIT construction procedure can be described as follows:

1) For the ith reference facet, generate the angular space.

2) Divide the angular space into a set of N_a modified angular regions.

3) For the jth angular region, generate MAR_{ij}.

4) Find relative facets in MAR_{ij}.

5) Construct MDIT, $TABLE(i, j, k)$ which contains the relative facets obtained in step 4 ($i = 1, 2, \ldots, N; j = 1, 2, \ldots, N_a, k = 1, 2, \ldots, N_r$, where N is the number of facets modeling the target and N_r is the number of relative facets in each region).

6) Repeat steps 3 to 5 for all angular regions.

7) Repeat steps 1 to 6 for all reference facets.

MDIT construction requires checking whether the relative facets are within MAR_{ij}. Recall that the three-dimensional space enclosed by outermost edge planes and a reference facet is called MAR_{ij}. Therefore, the first step for checking the existence of relative facets within MAR_{ij} is as follows:

$$a_m x_n + b_m y_n + c_m z_n + d_m > 0, \quad \text{for all } n \tag{1}$$

where (x_n, y_n, z_n) $(n = 1, 2, 3)$ are the three vertices of the relative facet. The relative facets that satisfy (1) are outside of MAR_{ij}, which will be discarded from the MDIT. If the relation in (1) does not hold even for a single n, i.e., even for any single vertex of a relative facet, then the relative facet is considered as a candidate for being "the facet within MAR_{ij}".

The second step can further reduce the number of candidate facets using the following relation:

$$a_m x_n + b_m y_n + c_m z_n + d_m < 0, \quad \text{for all } m \tag{2}$$

In other words, among candidate relative facets filtered by (1), facets with any single vertex satisfying (2) should be included in the MDIT.

Only if candidate relative facets are selected by (1) but dropped by (2) does the third step perform complex intersection tests. Thus, MADA does not perform time-consuming intersection tests for all relative facets, but only for a small number of pre-filtered relative facets. The intersection test proceeds as follows (Figure 6):

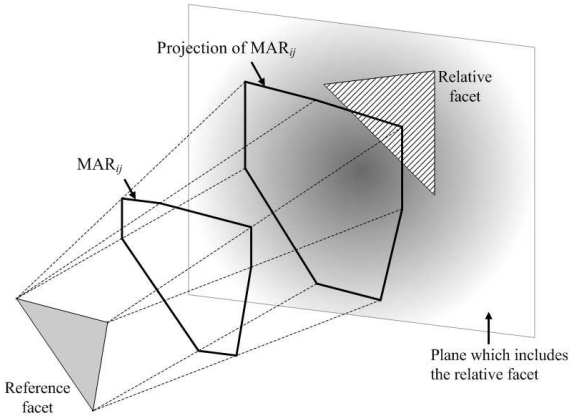

Figure 6. Intersection tests between the relative facet and MAR$_{ij}$.

1) Calculate the projection of MAR$_{ij}$ onto the plane which includes the relative facet.

2) Check whether an intersection between the relative facet and the projected polygon occurs using two-dimensional polygon set operations [6–8].

3) If any intersection occurs, the relative facet is within MAR$_{ij}$. Otherwise, the facet is not within MAR$_{ij}$.

The RCS prediction procedure using MADA is identical to that using ADA except the MDIT construction method. MADA can reduce the calculation time of SBR considerably without a loss of RCS prediction accuracy. The RCS prediction procedure is described as follows [21, 22]:

1) Model the target as a set of facets.

2) Construct MDIT, $TABLE(i, j, k)$.

3) Construct the incident ray tube grids.

4) Trace each ray tube.

5) Find the reflected facet and save its index number into A_i.

6) Calculate the direction of the reflected ray.

7) Find the angular region that the reflected ray goes into and save its index number into A_j.

8) Perform the intersection test between the ray and facets stored in $TABLE(A_i, A_j, k)$.

9) If the reflection occurs, save the index number of the reflected facet into A_i and go to step 6. Otherwise, terminate ray-tracing and perform the physical optics integral on the exit position.

10) Repeat steps 4 to 9 for all incident ray tubes.

4. RESULTS

In this paper, the monostatic RCS of two targets, simple dihedral and battleship model, were predicted to demonstrate the accuracy of the proposed method. RCS predictions were performed with a 1 degree increment. It was assumed that targets were made of a perfect electrical conductor and the maximum allowed reflection order was five.

The accuracy of the proposed MADA was compared with that of the conventional ADA using the dihedral model shown in Figure 7. Both the MADA and ADA simulations used 77 angular regions, as shown in Figure 8. The monostatic RCS of the dihedral target at a frequency of 5 GHz was computed in the azimuth and elevation planes shown in Figure 7 with MADA, ADA, and the conventional SBR, as shown in Figure 9. As shown in Figure 9(a), MADA and ADA showed good agreement with the conventional SBR in the azimuth plane. As mentioned earlier, MADA and ADA construct their tables with correct ϕ values, which allow the RCS values calculated by the two methods to be exactly identical to those calculated by the conventional SBR, as shown in Figure 9(a). However, in Figure 9(b), ADA had some prediction errors caused by the incorrect θ values. ADA calculated the maximum and the minimum ϕ angles between the reference facet labeled 1 and the relative facet labeled 7 to be 225° and 135°, respectively, and the maximum and the minimum θ angles were 45° and 35.3°. Thus, relative facet 7 was stored in four angular

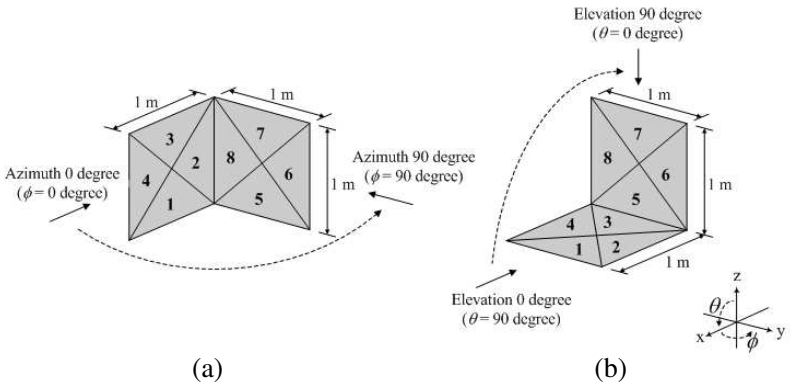

Figure 7. Simple dihedral model used in simulation: (a) azimuth plane and (b) elevation plane. Triangular facets are labeled with index numbers.

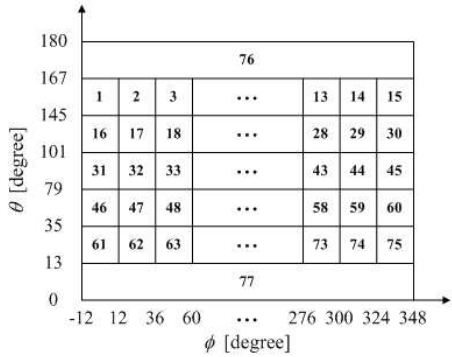

Figure 8. Definition of angular regions. Angular regions are labeled with index numbers.

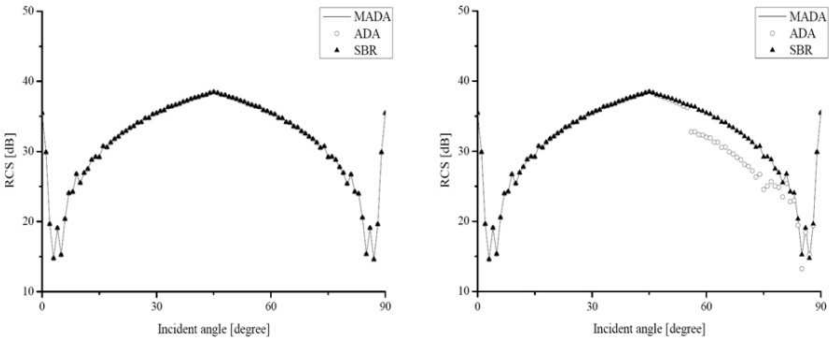

Figure 9. Monostatic RCS of the dihedral model.

regions, 52, 53, 54, and 55. The intersection tests between facet 7 and rays reflected from facet 1 were not performed when the reflected rays headed outside of those angular regions. However, the true minimum θ value is 26.6°. Therefore, the reflected ray from facet 1 missed the facet 7 when the ray had θ values between 26.6° and 35°, leading to the discontinuity at an elevation of 55° in Figure 9(b). In this simulation using a simple dihedral target, the conventional ADA can provide correct results if intersection tests were performed for angular regions 67, 68, 69, and 70. This can be achieved by changing the 35° θ boundary to 36° or greater.

A battleship model was also considered to demonstrate the accuracy of the proposed method (Figure 10). The target was modeled

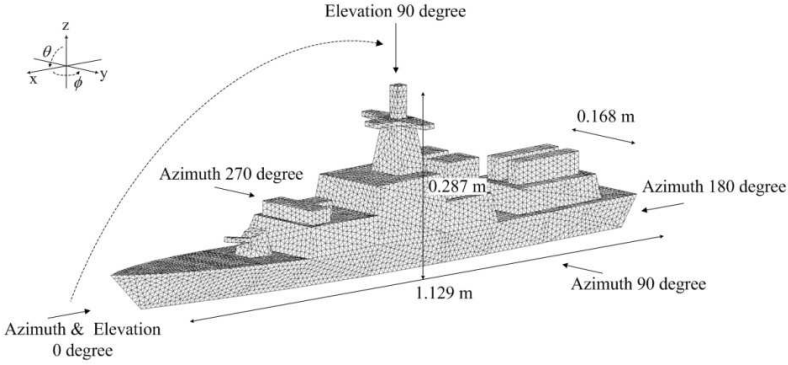

Figure 10. Angle planes and dimensions of the battleship model used in simulation.

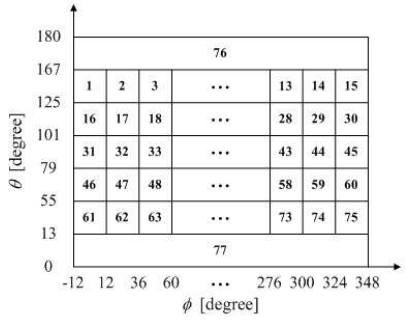

Figure 11. Definition of angular regions. Angular regions are labeled with index numbers.

with 8402 facets. The monostatic RCS of the target at a frequency of 10 GHz were predicted with the proposed MADA, the conventional ADA, and the conventional SBR in azimuth and elevation planes as illustrated in Figure 10. Both MADA and ADA simulations used 77 angular regions, as shown in Figure 11 to uniformly divide the angular space. In Figure 12, the RCS values calculated with the proposed MADA are exactly identical to those of the conventional SBR, while the relative RMS error between the conventional ADA and conventional SBR are 0.30 dB and 0.12 dB in the azimuth and elevation planes, respectively. The discrepancy between ADA and conventional SBR was caused by ray-misses for multiple reflections. Therefore, as multiple scattered fields from the target are more dominant than single reflection terms, this discrepancy may increase. If θ boundary

values of the angular regions shown in Figure 8 were changed, the ADA results shown in Figure 12 could be changed but still had some errors compared with SBR. However, the results from MADA had no error irrespective of θ boundary values. Moreover, accuracy of the results with ADA depend on the number of angular regions, the shape of targets or the number of facets modeling targets, while the results with MADA are always identical with those of the conventional SBR. The results in Figure 9 and Figure 12 show that the proposed MADA has better RCS prediction accuracy than the conventional ADA.

Computational complexities including times and table size are compared in Table 1 for the battleship model. The table construction of MADA, which is performed only once when the geometry of the target is given, requires more computation time than that of ADA because MADA requires a more complex table construction algorithm to fix the incorrect θ problems in ADA. Clearly, MADA and ADA perform much faster RCS predictions than conventional SBR. MADA required slightly more computation time than ADA.

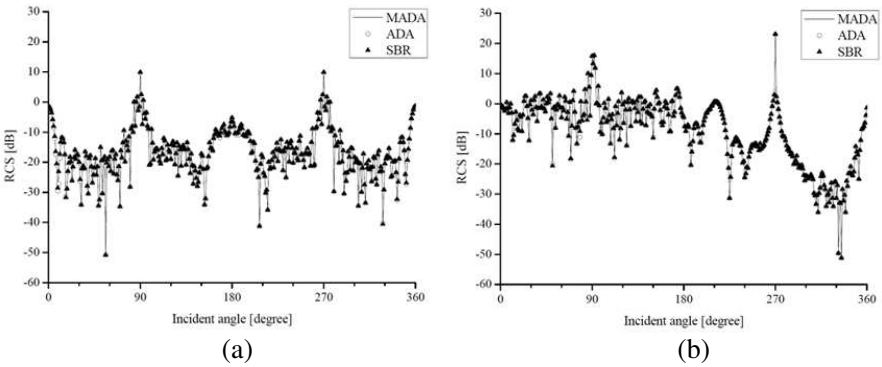

Figure 12. Monostatic RCS of the battleship model: (a) azimuth plane and (b) elevation plane.

Table 1. The calculation time, table size, and table construction time for the battleship model.

Methods	Ray tracing time [sec]		Table size [MB]	Table construction time [sec]
	Azimuth	Elevation		
SBR with MADA	413.994	312.161	28.31	272.503
SBR with ADA	413.880	306.929	29.16	218.037
Conventional SBR	4174.380	5504.620	-	-

As aforementioned, MADA performed intersection tests without ray-miss, unlike the conventional ADA. This can lead to more intersection tests, taking more computation time. However, it is noteworthy that MADA can achieve an RCS prediction accuracy comparable to the conventional SBR with much less computation time.

5. CONCLUSION

In this paper, MADA has been proposed to improve the accuracy of the conventional ADA. The DIT of the conventional ADA is generated according to incorrect relative angular position between reference and relative facets, which gives rise to ray-miss problems for multiple reflections. MADA precisely defines the three-dimensional space where the reflected ray can propagate by MAR_{ij}. Then, a MDIT is constructed using the facets in MAR_{ij}. Thus, MADA can provide more accurate RCS predictions than conventional ADA. Simulation results show that MADA can achieve good RCS predictions accuracy with much less computation time than the conventional SBR.

ACKNOWLEDGMENT

This work was supported by the Brain Korea 21 Project in 2011.

REFERENCES

1. Garcia-Donoro, D., I. Martinez-Fernandez, L. E. Garcia-Castillo, Y. Zhang, and T. K. Sarkar, "RCS computation using a parallel in-core and out-of-core direct solver," *Progress In Electromagnetics Research*, Vol. 118, 505–525, 2011.
2. Klement, D., J. Preissner, and V. Stein, "Special problems in applying the physical optics method for backscatter computation of complicated objects," *IEEE Trans. on Antennas Propag.*, Vol. 36, No. 2, 228–237, 1988.
3. Ling, H., R. C. Chou, and S. W. Lee, "Shooting and bouncing rays: Calculating the RCS of an arbitrarily shaped cavity," *IEEE Trans. on Antennas Propag.*, Vol. 37, No. 2, 194–205, 1989.
4. Suk, S.-H., T.-I. Seo, H.-S. Park, and H.-T. Kim, "Multiresolution grid algorithm in the SBR and its application to the RCS calculation," *Microw. Opt. Tech. Lett.*, Vol. 29, No. 6, 394–397, 2001.

5. Gao, P. C., Y. B. Tao, and H. Lin, "Fast RCS prediction using multiresolution shooting and bouncing ray method on the GPU," *Progress In Electromagnetics Research*, Vol. 107, 187–202, 2010.
6. Park, H.-G., H.-T. Kim, and K.-T. Kim, "Beam tracing for fast RCS prediction of electrically large targets," *Progress In Electromagnetics Research M*, Vol. 20, 29–42, 2011.
7. Tao, Y. B., H. Lin, and H. J. Bao, "Adaptive aperture partition in shooting and bouncing ray method," *IEEE Trans. on Antennas Propag.*, Vol. 59, No. 9, 3347–3357, 2011.
8. Heckbert, P. S. and P. Hanrdahan, "Beam tracing polygonal objects," *Computer Graphics (Proc. SIGGRAPH)*, Vol. 18, No. 3, 119–127, 1984.
9. Teh, C. H. and H. T. Chuah, "An improved image-based propagation model for indoor and outdoor communication channels," *Journal of Electromagnetic Waves and Applications*, Vol. 17, No. 1, 31–50, 2003.
10. Chung, B. K., C. H. Teh, and H. T. Chuah, "Modeling of anechoic chamber using a beam-tracing technique," *Progress In Electromagnetics Research*, Vol. 49, 23–38, 2004.
11. Di Giampaolo, E., M. Sabbadini, and F. Bardati, "Astigmatic beam tracing for GTD/UTD methods in 3-D complex environments," *Journal of Electromagnetic Waves and Applications*, Vol. 15, 439–460, 2001.
12. Di Giampaolo, E. and F. Bardati, "A projective approach to electromagnetic propagation in complex environments," *Progress In Electromagnetics Research B*, Vol. 13, 357–383, 2009.
13. Havran, V. and J. Bittner, "On improving kd-trees for ray shooting," *Proceedings of WSCG'2002 Conference*, 209–217, 2002.
14. Tao, Y. B., H. Lin, and H. J. Bao, "KD-tree based fast ray tracing for RCS prediction," *Progress In Electromagnetics Research*, Vol. 81, 329–341, 2008.
15. Glassner, A. S., "Space subdivision for fast ray tracing," *IEEE Computer Graphics and Applications*, Vol. 4, No. 10, 15–22, 1984.
16. Jin, K.-S., T.-I. Suh, S.-H. Suk, B.-C. Kim, and H.-T. Kim, "Fast ray tracing using a space-division algorithm for RCS prediction," *Journal of Electromagnetic Waves and Applications*, Vol. 20, No. 1, 119–126, 2006.
17. Bang, J.-K., B.-C. Kim, S.-H. Suk, K.-S. Jin, and H.-T. Kim, "Time consumption reduction of ray tracing for RCS prediction using efficient grid division and space division algorithms," *Journal of Electromagnetic Waves and Applications*, Vol. 21,

No. 6, 829–840, 2007.

18. Catedra, M. F., J. Perez, F. S. de Adana, and O. G. Blanco, "Efficient ray-tracing techniques for three-dimensional analyses of propagation in mobile communications: Application to picocell and microcell scenarios," *IEEE Antennas Propag. Mag.*, Vol. 40, 15–28, 1998.
19. De Adana, F. S., O. G. Blonco, I. G. Diego, J. P. Arriaga, and M. F. Catedra, "Propagation model based on ray tracing for the design of personal communication systems in indoor environments," *IEEE Trans. on Antennas Propag.*, Vol. 49, No. 6, 2105–2112, 2000.
20. Saeidi, C. and F. Hodjatkashani, "Modified angular z-buffer as an acceleration technique for ray tracing," *IEEE Trans. on Antennas Propag.*, Vol. 58, No. 5, 1822–1825, 2010.
21. Kim, B.-C., K.-K. Park, and H.-T. Kim, "Efficient RCS prediction method using angular division algorithm," *Journal of Electromagnetic Waves and Applications*, Vol. 23, No. 1, 65–74, 2009.
22. Park, K.-K. and H.-T. Kim, "RCS prediction acceleration and reduction of table size for the angular division algorithm," *Journal of Electromagnetic Waves and Applications*, Vol. 23, No. 11–12, 1657–1664, 2009.
23. Sedaghat Alvar, N., A. Ghorbani, and H. Amindavar, "A novel hybrid approach to ray tracing acceleration based on pre-processing & bounding volumes," *Progress In Electromagnetics Research*, Vol. 82, 19–32, 2008.
24. Sarker, M. S., A. W. Reza, and K. Dimyati, "A novel ray-tracing technique for indoor radio signal prediction," *Journal of Electromagnetic Waves and Applications*, Vol. 25, No. 8–9, 1179–1190, 2011.
25. Kim, H. and H.-S. Lee, "Accelerated three dimensional ray tracing techniques using ray frustums for wireless propagation models," *Progress In Electromagnetics Research*, Vol. 96, 21–36, 2009.
26. Liu, Z.-Y. and L.-X. Guo, "A quasi three-dimensional ray tracing method based on the virtual source tree in urban microcellular environments," *Progress In Electromagnetics Research*, Vol. 118, 397–414, 2011.
27. Reza, A. W., M. S. Sarker, and K. Dimyati, "A novel integrated mathematical approach of ray-tracing and genetic algorithm for optimizing indoor wireless coverage," *Progress In Electromagnetics Research*, Vol. 110, 147–162, 2010.

28. Gao, P. C., Y. B. Tao, Z. H. Bai, and H. Lin, "Mapping the SBR and TW-ILDCS to heterogeneous CPU-GPU architecture for fast computation of electromagnetic scattering," *Progress In Electromagnetics Research*, Vol. 122, 137–154, 2012.
29. Usai, P., A. Corucci, S. Genovesi, and A. Monorchio, "Arbitrary voxel selection for accelerating a ray tracing-based field prediction model in urban environments," *Progress In Electromagnetics Research C*, Vol. 20, 43–53, 2011.
30. Haarscher, A., P. de Doncker, and D. Lautru, "Uncertainty propagation and sensitivity analysis in ray-tracing simulations," *Progress In Electromagnetics Research M*, Vol. 21, 149–161, 2011.
31. Lim, H., J.-H. Park, J.-H. Yoo, C.-H. Kim, K. Kwon, and N.-H. Myung, "Joint time-frequency analysis of radar micro-doppler signatures from aircraft engine models," *Journal of Electromagnetic Waves and Applications*, Vol. 25, No. 8–9, 1069–1080, 2011.
32. Lim, H. and N.-H. Myung, "High resolution range profile-jet engine modulation analysis of aircraft models," *Journal of Electromagnetic Waves and Applications*, Vol. 25, No. 8–9, 1092–1102, 2011.
33. Gomez, J., A. Tayebi, F. M. Saez de Adana, and O. Gutierrez, "Localization approach based on ray-tracing including the effect of human shadowing," *Progress In Electromagnetics Research Letters*, Vol. 15, 1–11, 2010.
34. Zhang, Z. and W.-B. Dou, "A compact THz scanning imaging system based on improved reverse-microscope system," *Journal of Electromagnetic Waves and Applications*, Vol. 24, No. 8–9, 1045–1057, 2010.
35. Buddendick, H. and T. F. Eibert, "Bistatic image formation from shooting and bouncing rays simulated current distributions," *Progress In Electromagnetics Research*, Vol. 119, 1–18, 2011.